

Sequential hypothesis testing for Axion Haloscopes

Andrea GALLO ROSSO^{*1}, Sara ALGERI², and Jan CONRAD¹

¹Physics Department and Oskar Klein Centre, Stockholm University, Stockholm, Sweden

²School of Statistics, University of Minnesota, Minneapolis, MN, USA

Abstract

The goal of this paper is to introduce a novel likelihood-based inferential framework for axion haloscopes which is valid under the commonly applied “rescanning” protocol. The proposed method enjoys short data acquisition times and a simple tuning of the detector configuration. Local statistical significance and power are computed analytically, avoiding the need of burdensome simulations. Adequate corrections for the look-elsewhere effect are also discussed. The performance of our inferential strategy is compared with that of a simple method which exploits the geometric probability of rescan. Finally, we exemplify the method with an application to a HAYSTAC type axion haloscope.

1. Introduction

The existence of dark matter was first postulated almost a century ago Zwicky [1] and is today a well-established paradigm in astrophysics and cosmology. However, its detection and identification on a fundamental level is still one of the most investigated problems across all physical sciences [2–8]. Among the plethora of viable particle candidates which may constitute dark matter, axions are some among the most appealing ones. In fact, they were originally theorized in relation to the strong CP problem of fundamental physics [9–12]. Only later, physicists realized axions exhibit properties that are consistent with those of cold dark matter and their behavior is compatible with cosmological and astrophysical constraints [13–15] — see [16–18] for recent reviews.

At present, the experimental effort towards a direct detection is witnessing many experiments being planned or already running [19–24]. One of the most well-established way to search for axions is through cavity microwave experiments, generally referred to as haloscopes. The idea was first proposed by Sikivie in 1985 [25]; it relies on the Primakoff effect [26] to induce the axion-to-photon conversion in a resonant apparatus by matching the Compton wavelength of the axion and the resonant mode of the cavity. The interaction appears as power being deposited at a frequency matching the axion mass, i.e. $\nu_a = m_a c^2 h^{-1}$.

Since the axion frequency ν_a is unknown *a priori*,

a standard axion experiment is conceptually run by sequentially tuning the detector over the available frequencies. The goal is that of identifying a peak emerging from the fluctuations in the noise power of the system. The ratio between the power deposited by the axion over the noise power determines the signal-to-noise ratio, which is directly linked to the sensitivity and improves with the time invested measuring. As a result, the extent to which an axion experiment is able to explore the parameter space does not depend just on the detector properties and the available resources, such as the total lifetime, but also on the way those resources are effectively allocated. In fact, while experimenters could (in principle) focus solely on one specific frequency and increase the signal-to-noise ratio arbitrarily, they have also the freedom to carefully evaluate the fluctuations measured over multiple frequencies and repeat the measurement only for those those deemed to provide promising hints of an axion. It follows that the choice of such protocol for both data acquisition and statistical analyses is crucial.

Despite a variety of protocols have been proposed [e.g., 27–30], the main source of disagreement across different experiments is how to flag plausible candidate frequencies to be rescanned. This especially true when aiming to perform an analysis in a frequentist framework.

In this manuscript, we aim to address this inconsistency by introducing a statistically rigorous, likelihood-based, rescan protocol which provides the tools needed for a direct comparison of the results of

*andrea.gallo.rosso@fysik.su.se.

future experiments, such as the reachable sensitivity, or upper limits on the axion-photon coupling. We believe that this is especially needed given that there is no general consensus on the way such quantities are defined within the community.

The proposed inferential framework is presented in Sections 2-4. In order to ease the exposition, the main elements of the procedure are introduced in a step-by-step manner, gradually increasing level of complexity. Specifically, in Section 2, we outline the frequentist likelihood-based approach for axion searches in the simple scenario where only one scan is performed at a given frequency. In Section 3, we introduce the re-scan protocol, i.e., we allow our measurements to be conducted sequentially, over multiple scans at a fixed frequency. This is the main methodological result of the article. In Section 4, we discuss adequate “look-elsewhere effect” (LEE) corrections. That is, we allow the re-scan protocol to be performed over multiple frequencies. Hence, adequate LEE adjustments are introduced in order to control the probability of a false discovery over the entire frequency range considered. Section 5 outlines how to set upper limits in the context of a real axion experiment. Specifically, we use the parameterized properties of the first phase of HAYSTAC detector [31, 32] to make a projection of the reachable upper limit on the photon-axion coupling constant, showing how different definitions can affect the final result. A summary and concluding remarks are presented in Section 6.

2. Likelihood-based inference

In what follows, we assume that the sensitivity domain of a given axion experiment is discretized into M bins, each one of them marking a frequency ν_i , indexed by the subscript $i = 1, \dots, M$. The measuring process associates to the i -th bin a set of y_{ij} normalized noise fluctuations, possibly taken under different detector configurations $j = 1, \dots, N_i$. We assume the fluctuations y_{ij} to be normally distributed with unknown mean, μ_{ij} , and known standard deviation, σ_{ij} , i.e.,

$$y_{ij} \sim \mathcal{N}(\mu_{ij}, \sigma_{ij}). \quad (1)$$

The normality assumption in (1) simplifies the calculations and is a reasonable approximation of the true distribution of the noise fluctuations [e.g., 33–35]. In Equation (1), the mean μ_{ij} is nonzero only if an axion deposits power proportional to some coupling, A , on the i -th frequency bin, i.e.,

$$\mu_{ij} = A w_{ij}. \quad (2)$$

Here, A is the parameter of interest and the weights w_{ij} are assumed to be known — see for instance Equa-

tion (42) in Section 5 or Ref. [36]. The main goal of the proposed analysis is that of testing the hypotheses

$$H_0 : A = 0 \quad \text{versus} \quad H_1 : A \neq 0; \quad (3)$$

that is, we aim to assess if the *null hypothesis*, H_0 , of no axion is consistent with the observations collected by the detector.

Denote with $Y_t = \{y_{i1}, \dots, y_{iN_i}\}_{i \in \mathcal{I}_t}$ the sets of fluctuations relevant to check for the presence of an axion at a frequency ν_t , with $t = 1, \dots, T$, and $T \leq M$. Specifically, Y_t collects all the normalized noise fluctuations measured across all the N_i detector configurations at frequencies ν_i in a neighborhood \mathcal{I}_t of ν_t . From (1) it follows that the likelihood function is

$$\mathcal{L}_t(A) = \prod_{i \in \mathcal{I}_t} \prod_{j=1}^{N_i} \phi(y_{ij}; Aw_{ij}, \sigma_{ij}), \quad (4)$$

where $\phi(\cdot; Aw_{ij}, \sigma_{ij})$ denotes the density of a normal with mean Aw_{ij} and standard deviation σ_{ij} .

We begin by investigating the case where the presence of an axion is tested at a given frequency ν_t . In order to simplify the notation, the subscript t is dropped in the remainder of this section and in Section 3. It will be reintroduced in Section 4, when discussing the situation where multiple tests conducted simultaneously over different frequencies.

The statistic we rely upon to test (3) is the *signed-root likelihood ratio test* [e.g., 37]. When testing the hypotheses in (3), it specifies as

$$s = \frac{x}{\sqrt{u}}, \quad (5)$$

where

$$x = \sum_{i \in \mathcal{I}} \sum_{j=1}^{N_i} \frac{w_{ij} y_{ij}}{\sigma_{ij}^2} \quad \text{and} \quad u = \sum_{i \in \mathcal{I}} \sum_{j=1}^{N_i} \frac{w_{ij}^2}{\sigma_{ij}^2}. \quad (6)$$

Here, u summarizes the various detector configurations, with no need to further transform and rescale the original data y_{ij} , which are now aliased by the (one-dimensional) random variable x . Being a linear combination of normally distributed random variables, x is also Gaussian with variance $\sigma_x^2 = u$ and mean $\mu_x = Au$. The latter is valid assuming the most favorable case, i.e. the hypothesis of an axion lying on the frequency being tested. In fact, we may expect that, on a given frequency bin, an axion with (true) frequency ν_a and coupling constant A deposits the same power of an axion with (slightly shifted) frequency ν'_a and coupling constant $A' = Aw'_{ij}/w_{ij}$.

Under H_0 in (3), the distribution of the test statistic s in (5) is that of a standard normal. Whereas, if H_0

is false, then a mean shift is introduced. Once an experimental value \hat{s} is measured, the significance of the departure from the null hypothesis of zero mean can be quantified by computing the p-value

$$P(s \geq \hat{s} | H_0) = 1 - \Phi(\hat{s}), \quad (7)$$

where $\Phi(\cdot)$ is the cumulative distribution function of a standard Gaussian. When the probability (7) is below a pre-determined significance, typically denoted by α , then H_0 is rejected and a discovery is claimed. Conventionally, the line is drawn at 5σ significance which corresponds to $\alpha = 1 - \Phi(5) = 2.87 \times 10^{-7}$. In the following, we will refer to this as the *statistical discovery* condition, neglecting any additional procedure such as the “manual interrogation” of persistent candidates [34, 35].

3. The rescan protocol

We now extend the experimental freedom by introducing the option to flag promising noise fluctuations as potential candidates, and increase the data sample with subsequent measurements. Additional measurements are done sequentially, until the fluctuation disappears or a discovery is claimed. Here, we will consider two main methods, the so-called *geometric test* (and adequate generalizations), and our *likelihood-based rescan protocol*. As it will become clear in Sections 3.1-3.2, the former is essentially equivalent to the frequentist framework discussed in [29], whereas the latter is new, and allows us to include additional information into the analysis.

3.1. The geometric approach

A rather simple procedure to test for the presence of an axion is sketched in Figure 1. The inputs required are the desired significance level, α , needed to claim a discovery, and the probability of performing an additional scan.

Specifically, denote with $y_{ij\ell}$ the fluctuation measured on bin i , under the j -th detector configuration during the ℓ -th session of measurement, or rescan. Let x_ℓ be the value of x in (6) observed at the ℓ -th scan, i.e.,

$$x_\ell = \sum_{i \in \mathcal{I}} \sum_{j=1}^{N_i} \frac{w_{ij\ell} y_{ij\ell}}{\sigma_{ij\ell}^2}. \quad (8)$$

Similarly to Section 2, we assume that the x_ℓ are independent and normally distributed with mean depending on the coupling constant A , i.e., $\mu_{x_\ell} = Au_\ell$, and variance

$$u_\ell = \sum_{i \in \mathcal{I}} \sum_{j=1}^{N_i} \frac{w_{ij\ell}^2}{\sigma_{ij\ell}^2}. \quad (9)$$

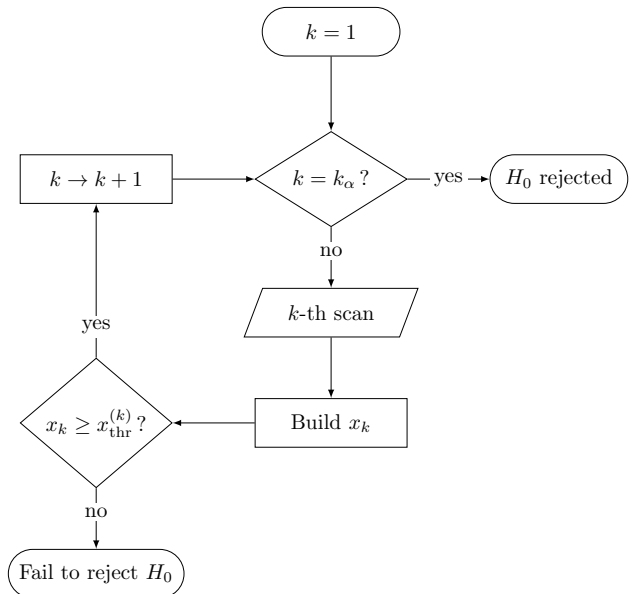


Figure 1: Flowchart of the rescan protocol based on the geometric test (Section 3.1). Its outcomes are either success (or fail) in rejecting H_0 and claiming (or not) the axion discovery.

The $(\ell + 1)$ -th scan is performed if the condition

$$x_\ell > x_{\text{thr}} \quad (10)$$

is verified for some pre-determined threshold x_{thr} . The latter can be chosen, for example, to ensure that the probability of rescan when no axion is present (under H_0) is 5%, i.e.,

$$P(x_\ell > x_{\text{thr}} | H_0) = 0.05. \quad (11)$$

We then proceed by considering the total number of scans being performed, K , as our test statistic. Specifically, (10) implies that additional measurements are collected until such conditions no longer holds. Hence, K can be treated as a geometric random variable with probability of “success” given by the complement of (11). Notice that, in this context a “success” corresponds to the even of stopping the procedure. We can then reject the null hypothesis of “no axion” whenever the rescan protocol based on (10) leads to k scans, with k satisfying

$$P(K \geq k | H_0) = [P(x_\ell > x_{\text{thr}} | H_0)]^{(k-1)} \leq \alpha. \quad (12)$$

Notice that K differs from k in that the former is a random variable taking values $k \in \{1, \dots, \infty\}$. Therefore, the number k of rescans reached in a given experiment is simply the value of K observed.

The geometric test above can be further extended by allowing the threshold x_{thr} to vary at each scan.

This effectively reduces to the frequentist approach discussed in Ref. [29] and for which (12) generalizes to

$$P(K \geq k) = \prod_{\ell=1}^{k-1} \left[P(x_\ell > x_{\text{thr}}^{(\ell)} | H_0) \right] \leq \alpha \quad (13)$$

with $x_{\text{thr}}^{(\ell)}$ denoting the pre-determined threshold for the ℓ -th scan.

It is worth emphasizing that (12)-(13) allow us to determine the minimum number of scans, hereafter denoted by k_α , needed to claim a discovery at the prescribed significance level, α , and for a given set of threshold(s) $x_{\text{thr}}^{(\ell)}$. Alternatively, when the resources available strongly limit the maximum number of measurements that can be performed, one can tune the threshold(s) $x_{\text{thr}}^{(\ell)}$ to ensure that (13) is verified for a pre-determined value of k_α .

3.2. The likelihood-based rescanning protocol

Despite the simplicity of the approach outlined in Section 3.1, its main limitation is that it requires us to perform at least $k_\alpha - 1$ measurements in order to claim a statistical discovery. Moreover, as noted in [29], a design based on binary outcomes like (10) is blind to the actual magnitude of the fluctuations, leading to a waste of potentially valuable information. Here, we outline a novel procedure which allows us to overcome these limitations. Additional advantages in terms of power and number of rescans needed to claim a statistical discovery are discussed in Section 3.3.

The main steps of our proposed procedure are summarized in Figure 2. We refer to this approach as *likelihood-based rescanning protocol* and it consists of the following.

Let k_α be the maximum number of scan to be performed. For example, as noted at the end of Section 3.1, k_α can be chosen on the basis of the resources available, or to ensure a significance level of α using the geometric approach. Recall that Y_h denotes the set of fluctuations relevant to check for the presence of an axion at a frequency ν_t in the h -th scan. At the ℓ -th scan, $\ell = 1, \dots, k_\alpha$, we compute the test statistic s_ℓ considering the set of measurements, $\bigcup_{h=1}^{\ell} Y_h$. The updated test statistic s_ℓ generalizes s in (5) in that

$$s_\ell = \frac{\sum_{h=1}^{\ell} x_h}{\sqrt{\sum_{h=1}^{\ell} u_h}}, \quad (14)$$

with x_h and u_h calculated as in (8) and (9), respectively, for each of the $h = 1, \dots, \ell$ scans. We then rely on two conditions to determine whether or not a statistical discovery should be claimed, or if an additional scan should be performed.

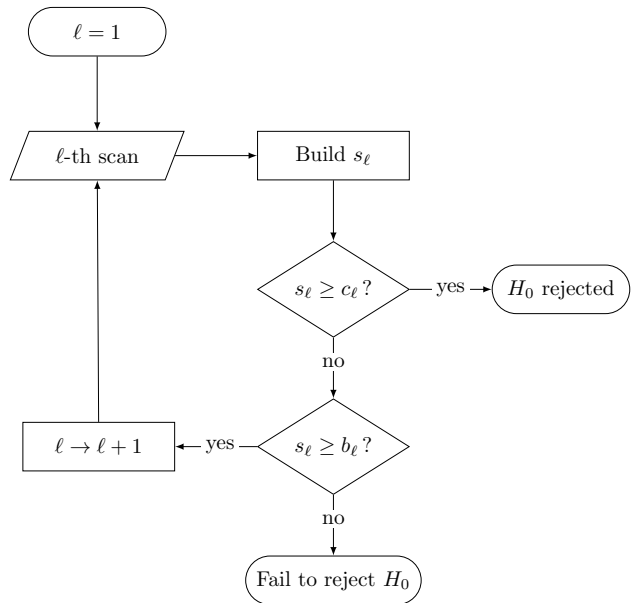


Figure 2: Flowchart of the likelihood-based rescanning protocol discussed in Section 3.2. The possible outcomes are the same as the geometric test (Figure 1).

Specifically, for a suitably chosen set of constants $\{c_\ell\}_{\ell=1}^{k_\alpha}$, once the ℓ -th scan has been completed, we first assess if the condition

$$C_\ell = \{s_\ell \geq c_\ell\} \quad (15)$$

is verified. If it is, a discovery claim is made. Whereas, if C_ℓ does not hold, we verify the validity of the condition

$$B_\ell = \{s_\ell \geq b_\ell\}, \quad (16)$$

where b_ℓ is the ℓ -th elements of a set of constants $\{b_\ell\}_{\ell=1}^{k_\alpha}$, used to control the probability of rescanning. If B_ℓ in (16) holds, we proceed with another rescanning; if B_ℓ is not verified, the experiment is stopped, and we declare no discovery. Note that in (15) and (16) we are implicitly setting $b_\ell \leq c_\ell$, with equality holding for $\ell = k_\alpha$ in order to have a definite outcome. It follows that, in our likelihood-based protocol, condition (16) plays the same role as (10) in the geometric approach. Conversely from the latter, however, by combining B_ℓ and C_ℓ , we allow researchers to claim a statistical discovery at any step, determining a potential break in the procedure even before reaching the k_α -th scan.

Clearly, the statistical validity of the proposed strategy depends entirely on the specification of the constants b_ℓ and c_ℓ . These must be chosen to ensure that the probability of a false discovery over multiple scans is no lower than the pre-determined significance level α . This can be done as follows.

Denote with D_ℓ the event of claiming a statistical discovery at the ℓ -th scan. On the basis of the scheme

in Figure 2, such event specifies as

$$D_\ell = \left[\bigcap_{h=1}^{\ell-1} \{C_h^c \cap B_h\} \right] \cap C_\ell, \quad (17)$$

with $C_h^c = \{s_h < c_h\}$. To ensure that the probability of a false discovery is indeed equal to the desired level α , we must guarantee that

$$P\left(\bigcup_{\ell=1}^{k_\alpha} D_\ell \middle| H_0\right) = \sum_{\ell=1}^{k_\alpha} P(D_\ell | H_0) = \alpha, \quad (18)$$

where the first equality follows from the fact that the events D_ℓ are mutually exclusive, i.e. their intersection is empty. Therefore, it is sufficient to choose b_ℓ and c_ℓ such that

$$P(D_\ell | H_0) = \frac{\alpha}{k_\alpha} \quad (19)$$

for all $\ell = 1, \dots, k_\alpha$ to ensure that (18) holds.

Interestingly, condition (19) can easily be expressed in closed form and thus one can exploit the latter to derive the constants b_ℓ and c_ℓ sequentially.

Specifically, for $\ell = 1$, the setup is the same as that outlined in Section 2. From (7), it follows that

$$P(D_1 | H_0) = P(s_1 \geq c_1 | H_0) = 1 - \Phi(c_1) = \frac{\alpha}{k_\alpha}, \quad (20)$$

and thus, c_1 is simply the quantile of order $1 - \alpha$ of a standard normal. The threshold b_1 , can be determined by solving the equation

$$\int_{b_1}^{c_1} ds_1 \mathcal{N}(s_1 | 0, 1) = q_1, \quad (21)$$

where q_1 is the probability of engaging in the second scan under the background-only hypothesis. For example, similarly to (11), we may chose $q_1 = 0.05$.

Let us extend the reasoning to the less trivial case of $\ell > 1$. Since the constants b_ℓ and c_ℓ are computed sequentially, it follows that, at the ℓ -th scan, b_h and c_h are known for all $h \leq \ell - 1$. Define $\mathbf{x} = (x_1, x_2, \dots, x_\ell)$ to be the vector of powers x_h computed as in (8) for each of the ℓ scans. Similarly, denote with $\mathbf{u} = (u_1, u_2, \dots, u_\ell)$ the vector collecting the respective configurations u_h in (9). Analogously, we can define the vector of test statistics $\mathbf{s} = (s_1, s_2, \dots, s_\ell)$, each computed as in (14). We can then easily derive the joint probability density function (pdf) of the random vector \mathbf{s} starting from that of \mathbf{x} , and which follows a multivariate normal of dimension ℓ , i.e.,

$$\mathbf{x} \sim \mathcal{N}_\ell(\boldsymbol{\mu}_\mathbf{x}, \boldsymbol{\Sigma}_\mathbf{x}) \quad (22)$$

with

$$\boldsymbol{\mu}_\mathbf{x} = A\mathbf{u} \quad \text{and} \quad \boldsymbol{\Sigma}_\mathbf{x} = \text{diag}(\mathbf{u}). \quad (23)$$

Denote with \mathbf{J} the Jacobian of the transformation in (14) that allows us to link the vectors \mathbf{x} and \mathbf{s} . From (22), it follows that

$$\mathbf{s} \sim \mathcal{N}_\ell(\mathbf{s} | \boldsymbol{\mu}_\mathbf{s} = \mathbf{J}\boldsymbol{\mu}_\mathbf{x}, \boldsymbol{\Sigma}_\mathbf{s} = \mathbf{J}\boldsymbol{\Sigma}_\mathbf{x}\mathbf{J}^T). \quad (24)$$

Combining (24) and (19) we have

$$\begin{aligned} \frac{\alpha}{k_\alpha} &= P(D_\ell | H_0) = \\ P(s_\ell \geq c_\ell, b_{\ell-1} \leq s_{\ell-1} < c_{\ell-1}, \dots, b_1 \leq s_1 < c_1) &= \\ \int_{c_\ell}^{\infty} ds_\ell \int_{b_{\ell-1}}^{c_{\ell-1}} ds_{\ell-1} \dots \int_{b_1}^{c_1} ds_1 \mathcal{N}_\ell(\mathbf{s} | \mathbf{0}, \boldsymbol{\Sigma}_\mathbf{s}). \end{aligned} \quad (25)$$

Ultimately, c_ℓ is obtained by solving the equation in (25).

Whereas, to determine the threshold b_ℓ , we consider the conditional probability of the event $\{b_\ell \leq s_\ell < c_\ell\}$ given the outcome of the previous $\ell - 1$ scans (with no discovery break). We require such probability to be equal to the desired probability of rescan q_ℓ (e.g., $q_\ell = 0.05$, for all $\ell = 1, \dots, k_\alpha$), i.e.,

$$\begin{aligned} P\left(C_\ell^c \cap B_\ell \middle| \bigcap_{h=1}^{\ell-1} \{C_h^c \cap B_h\}, H_0\right) &= \\ P\left(\bigcap_{h=1}^{\ell} \{C_h^c \cap B_h\} \middle| H_0\right) / P\left(\bigcap_{h=1}^{\ell-1} \{C_h^c \cap B_h\} \middle| H_0\right) &= \\ \frac{\int_{b_\ell}^{c_\ell} ds_\ell \dots \int_{b_1}^{c_1} ds_1 \mathcal{N}_\ell(\mathbf{s} | \boldsymbol{\mu}_\mathbf{s}, \boldsymbol{\Sigma}_\mathbf{s})}{\int_{b_{\ell-1}}^{c_{\ell-1}} ds_{\ell-1} \dots \int_{b_1}^{c_1} ds_1 \mathcal{N}_{\ell-1}(\mathbf{s} | \boldsymbol{\mu}_\mathbf{s}, \boldsymbol{\Sigma}_\mathbf{s})} &= q_\ell, \end{aligned} \quad (26)$$

where the first equality follows from Bayes's theorem. Notice that in (26) the only unknown quantity is the constant b_ℓ .

Equation (26) allows a step-by-step determination of the first $k_\alpha - 1$ constants b_ℓ . The last one, b_{k_α} , is chosen to be equal to c_{k_α} in order ensure that a conclusion is reached in no more than k_α scans.

3.3. Likelihood-based vs. geometric approach

In order to acquire a deeper understanding of the advantages and disadvantages of these two approaches, we investigate their statistical properties by means of a toy example. Let the maximum number of scans

Table 1: Coefficients b_ℓ and c_ℓ satisfying (25) and (26) for the toy example described in Section 3.3.

ℓ	1	2	3	4	5
b_ℓ	1.9929	3.1810	4.0916	4.7943	4.8031
c_ℓ	5.3018	5.2967	5.2681	5.1820	4.8031

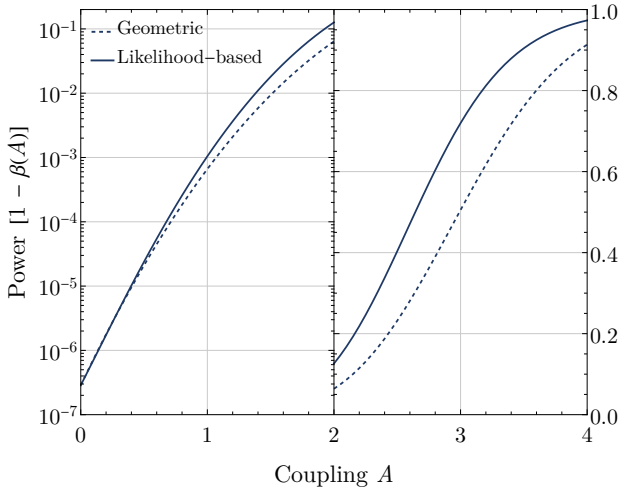


Figure 3: Power as a function of the coupling A . Dashed line: power for the geometric approach computed as in Equation (29). Solid line: power for the likelihood-based approach computed as in Equation (30). The values in the range $A \in [0, 2]$ are magnified in logarithmic scale.

to be performed by $k_\alpha = 5$ and consider the conventional 5σ level, that is, $\alpha = 2.8665 \times 10^{-7}$. For each $\ell = 1, \dots, k_\alpha$, we assume that $u_\ell = 1$ and we let

$$P(x_\ell > x_{\text{thr}} | H_0) = \alpha^{1/4}. \quad (27)$$

This would ensure that the probability of false discovery is exactly α , allowing a fair comparison of the power (see below and Figure 3). From condition (12), it follows that the threshold value, x_{thr} , for the geometric test is given by

$$x_{\text{thr}} = \Phi^{-1}(1 - \alpha^{1/4}) \approx 1.9929. \quad (28)$$

The b_ℓ and c_ℓ constants required by the likelihood-based rescan protocol have been computed as described in Section 3.2, with rescan probability as in (27). The resulting values of b_ℓ and c_ℓ are reported in Table 1.

We proceed by comparing the power of both approaches; that is, the probability to correctly reject the null hypothesis, H_0 in (3), when the alternative hypothesis, H_1 is true. In other words, the power corresponds to the sensitivity of our test in detecting an axion expressed in probabilistic terms. In statistical literature, it is conventionally denoted as $1 - \beta$, where β corresponds to the probability of type II error, i.e., the probability of failing to reject H_0 when H_1 is true. In our case, the power is a function of the coupling A constant and, for both the geometric and the likelihood-based rescan approach, it can be easily computed analytically. Specifically, for the geometric

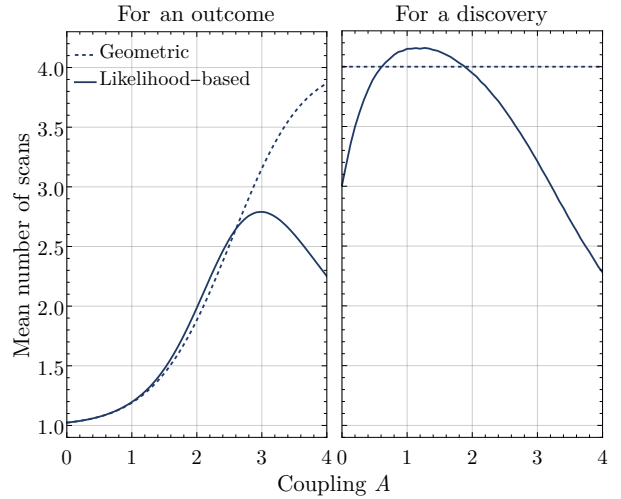


Figure 4: Mean number of scans needed to claim a statistical discovery (right) and to get an outcome, either a discovery or a no-discovery claim (left) for the two analysis approaches (Sections 3.1 and 3.2), for different values of the coupling A . The setup of the simulation is discussed in Section 3.3.

test, since $u_\ell = 1$, for all $\ell = 1, \dots, k_\alpha$, we have

$$1 - \beta(A) = [1 - \Phi(x_{\text{thr}} - A)]^{k_\alpha - 1}; \quad (29)$$

whereas, the power of the likelihood-based rescan protocol is

$$1 - \beta(A) = \sum_{h=1}^{k_\alpha} P(D_h | A). \quad (30)$$

In (30), the probabilities $P(D_h | A)$ can be calculated similarly to $P(D_h | H_0)$ in (25). The power functions in (29) and (30) are plotted in Figure 3.

As expected, since the likelihood-based protocol uses more information, it also exhibits higher power; especially for larger values of the coupling constant, A . The two methods perform similarly when A approaches zero.

We emphasize once more that this is a toy example used for illustrative purposes but with no realistic physical meaning. In general, the value of A is an alias for the coupling constant for the interaction channel under consideration and can carry units (see e.g. Section 5). For the same reason, the reachable sensitivity depends on the explicit values of u_ℓ (6), which can be constructed by tailoring the explicit configuration of a given detector. A fine tuning of the thresholds x_{thr} is also possible, in order to increase the power for smaller values of A . In this sense, analytic expressions (29) and (30) can be used to identify optimal choices of these parameters based on the specifics of the experiment being conducted.

Another useful aspect of the likelihood-based rescan protocol is that it does not require to perform all the k_α scans in order to claim a statistical discovery. Hence, it has the potential to reduce substantially the costs associated with additional rescans. Specifically, while a discovery claim via the geometric approach always requires us to perform $k_\alpha - 1$ scans (see Figure 1), on average, we may expect the average number of scans required for a statistical discovery to be approximately the same or lower for the likelihood-based rescan protocol. This is illustrated on the right panel of Figure 4 by means of a Monte Carlo simulation for our toy example. The left panel, shows that the average number of scans required to reach a conclusion (either a discovery or a no-discovery claim) is lowered when relying of the likelihood-based rescan protocol for large values of the coupling. Whereas, given the initial tuning, it is the same for both frameworks as $A \rightarrow 0$.

4. Look-elsewhere effect corrections

The protocols discussed in Section 3 can be meaningfully applied with no further modifications only when the interest is in testing *only one* given frequency. In the more realistic scenario where a set of $T \leq M$ frequencies $\{\nu_i\}_{i=1}^T$ is considered, the significance must be adjusted to account for the so-called *look-elsewhere effect* (LEE). That is, the probability that a random fluctuation may cross the discovery threshold anywhere over the frequency range considered. In other words, one must ensure that the probability of a false discovery at any frequency ν_1, \dots, ν_T does not exceed the desired significance level α .

While several solutions to address the LEE have been proposed in literature [e.g., 27, 38, 39], they are only applicable to the situation where just one scan is performed. In what follows, we discuss different approaches that allow us to correct for the LEE even when the data are collected sequentially over multiple scans.

The simplest possible solution is that of re-adapting classical approaches such as Šidák's and Bonferroni corrections [e.g., 38] to our context. This can be done by replacing α in (18) with $1 - (1 - \alpha)^{1/T}$ for Šidák and with α/T for Bonferroni. The former provides an exact result, but relies on the assumption that all the test being performed are independent. Whereas, the latter trades the assumptions of independence for a much more conservative result, and, consequently, lower power.

Unfortunately, in axion searches, the T tested frequencies are not independent. That is because the location of the axion is unknown, and thus, the step at

which the frequency range is scanned is usually smaller than the expected width of the signal. This is done to ensure that no power is shared between two regions and thus dampened. Nonetheless, one can overcome this limitation by implementing Šidák or Bonferroni corrections based on the effective number of independent regions, R_T^α . The latter can be defined as the value of independent tests that would determine the correct significance when replacing α in (18) with R_T^α (19) to compute the corresponding constants. Therefore, for a given value of R_T^α , an adequate LEE correction can be obtained by replacing the probability of a discovery claim under H_0 at the ℓ -th scan in (19) with

$$P(D_{t\ell}|H_0) = 1 - \left(1 - \frac{\alpha}{k_\alpha}\right)^{1/R_T^\alpha} \approx \frac{\alpha}{R_T^\alpha k_\alpha} \quad (31)$$

in order to have

$$\sum_{t=1}^T \sum_{\ell=1}^{k_\alpha} P(D_{t\ell}|H_0) = \alpha \quad (32)$$

for each of the frequencies, $t = 1, \dots, T$, being tested. Hereinafter, we will refer to this framework as the *independent regions* approach. In the latter, the number of independent regions, R_T^α , depends on both the number of scanned frequencies, T , and the significance level, α . Therefore, the procedure requires a Monte Carlo calibration of R_T^α on the basis of (32) — see e.g. [27].

Here, we propose an alternative solution that allows us to overcome all the limitations of the above-mentioned approaches. Our strategy consists of constructing an updated version of the constants c_ℓ that accounts for the LEE, while leaving the likelihood-rescan protocol (Figure 2) at each of the T frequencies unchanged. This can be done following the scheme on Figure 5; the main steps are described below.

For a given frequency, t , let L_t be the scan at which an outcome is reached when following the rescan-protocol in Section 3.2 and Figure 2. Denote with s_L^t the value of the test statistic at such scan; to ease the notation, the subscript t has been dropped from L_t since the dependency on frequency is reminded by the superscript. To control for the look-elsewhere effect we must guarantee that

$$P\left(\bigcup_{t=1}^T \{s_L^t - c_L^t \geq 0\} \middle| H_0\right) \leq \alpha, \quad (33)$$

which is equivalent to the condition

$$P\left(\max_{t=1, \dots, T} \{s_L^t - c_L^t\} > 0 \middle| H_0\right) \leq \alpha. \quad (34)$$

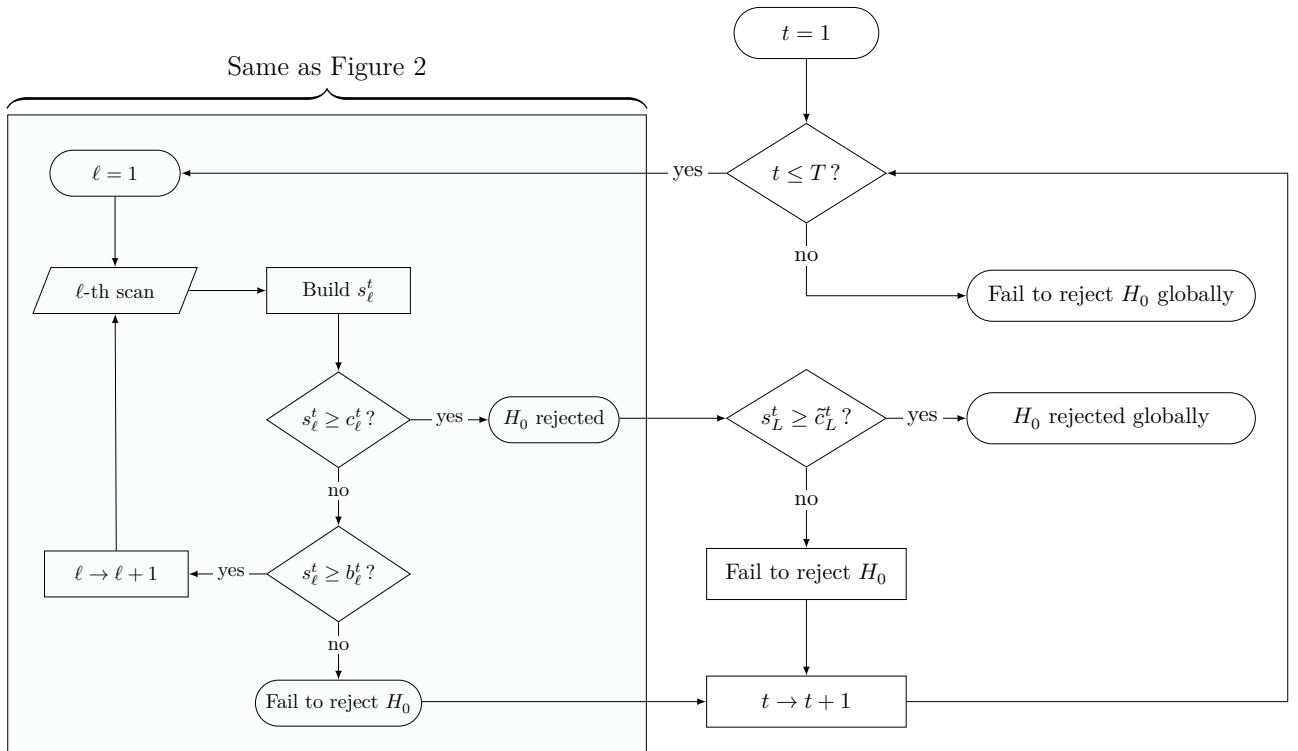


Figure 5: Flowchart of the likelihood-based rescanning protocol (Figure 2) corrected to account for the scan of multiple frequencies.

This leads to the definition of the new (global) statistic

$$\mathcal{S} = \max_{t=1, \dots, T} \{s_L^t - c_L^t\}. \quad (35)$$

which is simply the maximum of the stochastic process $\{s_L^t - c_L^t\}_{t=1}^T$. Notice that, while each s_ℓ in (14) is Gaussian, s_L^t is not; that is because its distribution depends on the (binary) outcome of the decision rule in (15), and thus the value L_t at which the decision is reached is itself random. Unfortunately, the distribution of \mathcal{S} cannot be easily derived explicitly, nor it can be approximated using the upcrossings/Euler characteristic heuristic typically used in the context of LEE corrections [39, 40]. Nonetheless, it is possible to retrieve the null distribution of \mathcal{S} by means of a Monte Carlo simulation.

Specifically, we are interested in estimating the quantile of order $1 - \alpha$ of \mathcal{S} , i.e. $\mathcal{S}_{1-\alpha}$ for which

$$P(\mathcal{S} > \mathcal{S}_{1-\alpha}) = \alpha.$$

We can then construct our newly “LEE-updated” constants, namely \tilde{c}_L^t , as

$$\tilde{c}_L^t = c_L^t + \mathcal{S}_{1-\alpha}. \quad (36)$$

Finally, a statistical discovery at (global) α significance is claimed if $s_L^t \geq \tilde{c}_L^t$ for at least one frequency

$t = 1, \dots, T$. The main steps of this approach are summarized in Figure 5.

4.1. Statistical properties of different LEE corrections

In this section, we investigate the properties of the look-elsewhere corrections described above by extending the toy example introduced in Section 3.3 to allow an analysis over multiple frequencies. Specifically, we start once again by considering a 5σ significance level ($\alpha = 2.87 \times 10^{-7}$) and $k_\alpha = 5$, so that the constants b_ℓ and c_ℓ are those reported in Table 1. The setup con-

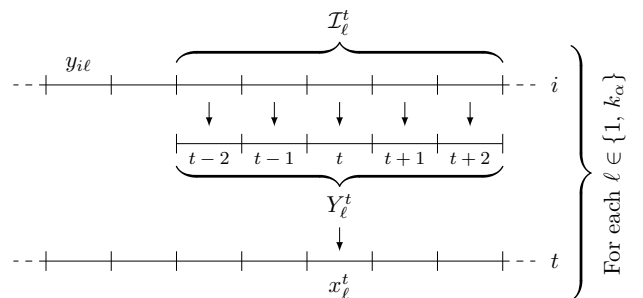


Figure 6: Scheme of the setup assumed in the toy example of Section 4.1.

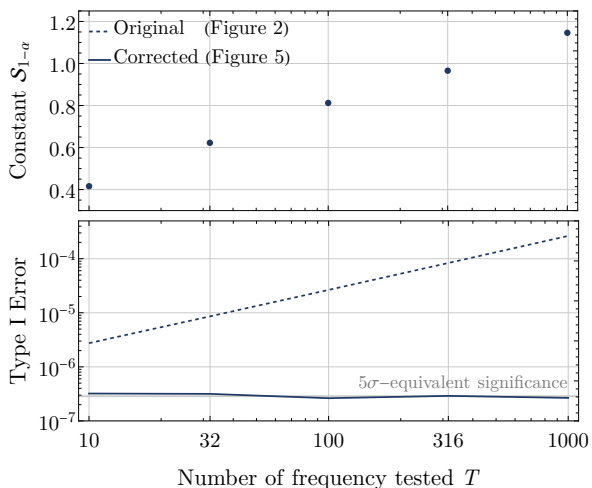


Figure 7: Top: Quantile of order $1-\alpha$ of the test statistic S in (35), as a function of the different number of frequencies T tested. Bottom: Probabilities of false discoveries for the proposed LEE corrections based on (36) (solid line) and those obtained when conducting only a localized analyses at each individual frequency with no LEE correction (dashed line).

sidered is illustrated in Figure 6, and is intended to emulate as closely as possible a real axion experiment.

The data consist of a string of noise fluctuations $y_{i\ell}$, with the index i marking the frequency ν_i at which the datum is taken; the subscript $\ell = 1, \dots, k_\alpha$ indexes the rescan. For simplicity, we consider only one detector configuration, i.e., $N_i = 1$ for all $i = 1, \dots, M$, and thus the subscript j is dropped.

We assume that $y_i \sim \mathcal{N}(\mu_i = 0, \sigma_i = 1)$, under H_0 . Whereas, the alternative hypothesis, H_1 , corresponds to a signal $\mu_i = A$, spanning over the neighborhood \mathcal{I}_ℓ^t of ν_t . The latter consists of a row of $d = 5$ frequency bins centered around ν_t . For each frequency ν_t , $t = 1, \dots, T$, being tested, the respective set of fluctuations Y_ℓ^t is collected over \mathcal{I}_ℓ^t . The quantities $x_\ell^t = \sum_{i=t-2}^{t+2} y_{i\ell}$ are then computed; whereas, the variances u_ℓ^t are constant and equal to $1/5$ for each $t = 1, \dots, T$ and $\ell = 1, \dots, k_\alpha$. Once an outcome is reached, ν_t is shifted by one bin and the procedure is repeated. Notice, once again, that $Y_\ell^t \cap Y_\ell^{t+1} \neq \emptyset$, thus the corresponding x_ℓ^t and x_ℓ^{t+1} (and the respective tests) are not independent.

We implement the LEE corrections based on (36) where the quantile $S_{1-\alpha}$ is estimated by means of a Monte Carlo simulation. The results obtained considering an increasing number of total frequencies, T , being tested are shown in the upper panel of Figure 7.

The bottom panel of Figure 7 shows that the LEE corrections based on (36) (solid line) ensure that the probability of false discovery is equal to the predeter-

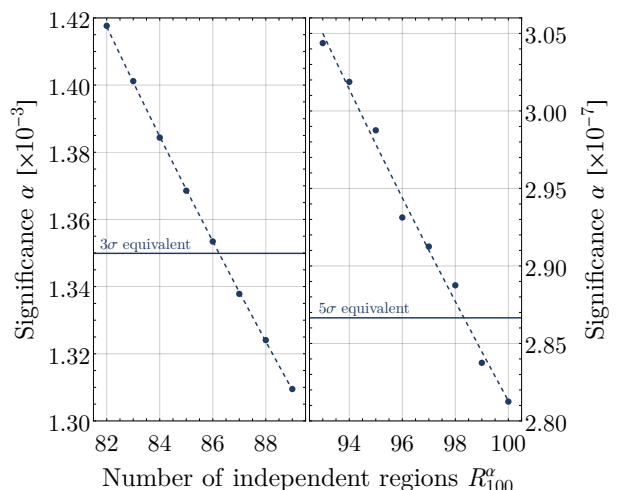


Figure 8: Probability of false discovery evaluated via Monte Carlo, when testing $T = 100$ frequencies at 3σ equivalent significance (left) and 5σ (right), as a function of independent regions R_{100}^α considered.

mined 5σ significance level. The same is not true when ignoring the LEE and conducting a local analysis at each individual frequency (dashed line). In this case, the probability of a false discovery increases with the number of tested frequencies.

For the sake of comparison, we also implement the LEE corrections based on the number of independent regions R_T^α (see Equation (31)). In this case, it is necessary to “tune” R_T^α by means of a Monte Carlo simulation. Figure 8, shows the probability of false discovery obtained when testing $T = 100$ frequencies. Recall that, in this case, the analytical framework is the same as that in Figure 2 with the constants c_ℓ and b_ℓ computed by assuming different values of R_T^α in order to ensure the validity of (31). On the left panel of Figure 8, we consider a significance level of 3σ , while the right panel corresponds to 5σ . When choosing $R_T^\alpha = T = 100$ the result is conservative (sensitivity loss); whereas, as R_T^α decreases the more we are susceptible to noise-triggered false claim. A linear fit applied to the Monte Carlo output shows that the number of independent region is $R_{100}^{5\sigma} \approx 98.3$ for a 5σ significance while it is sensibly lower in the 3σ case: $R_{100}^{3\sigma} \approx 86.2$.

Figure 9 compares the power of the LEE corrections based on (36) and those based on the independent regions approach at 3σ significance. Among the two, the independent region approach clearly enjoys higher power. This may be due to different reasons. Firstly, the procedure based on the independent regions lacks of what we may call “dangling outcomes”. That is, in the LEE framework of Figure 5, we may encounter the

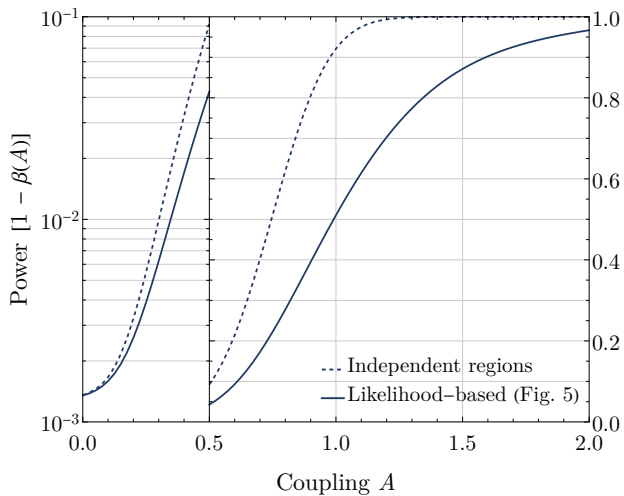


Figure 9: Power as a function of the coupling A for a significance of 3σ . Solid line: Corrected likelihood-based approach (Figure 5). Dashed line: likelihood-based approach (Figure 2) with $R_{100}^{3\sigma} \approx 86.2$ independent regions — see (31). The values in the range $A \in [0, 0.5]$ are magnified in logarithmic scale.

situation where

$$c_L^t \leq s_L^t < \tilde{c}_L^t. \quad (37)$$

In this case, the procedure stops and no discovery is claimed, even if the tested frequency has not been ruled out as a promising candidate. In fact, if only s_L^t had fluctuated below \tilde{c}_L^t (and $L < k_\alpha$) further scans would have been performed. Clearly, we may expect condition (37) to be in the “gray zone” between a very weak and very strong coupling. If $A \rightarrow 0$, we expect $s_L^t < b_L^t < c_L^t$ most of the times; whereas, if $A \rightarrow \infty$, we expect $s_L^t \gg \tilde{c}_L^t$.

As highlighted in Figure 10, the higher power reached by the independent-region procedure is also due to its tendency to perform more scans. In terms of number of scans needed, a peak is achieved in the transition between low to high powers (see e.g. left panel of Figure 10). The maximum difference in the number of scans per outcome occurs at approximately $A = 1$ and corresponds to the highest relative difference between the two powers. In other words, the power increases with the number of performed scans, which is not surprising.

Everything highlighted so far applies to the case of a toy example. In a real experiment, the inferential procedure adopted needs to be tailored on the specific setup to which it is applied. Moreover, the performance of different approaches is bounded by practical constraints such as measurement time, sensitivity reach, or tuning. A direct comparison among them

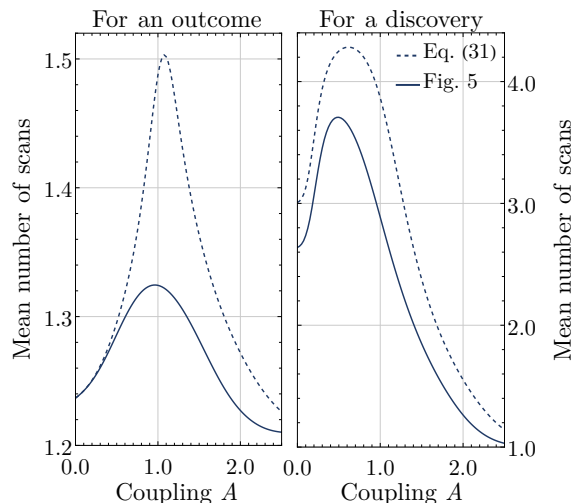


Figure 10: Mean number of scans needed to claim a statistical discovery (right) and to get an outcome, either a discovery or a no-discovery claim (left) for the approach outlined in Figure 5 (solid) and the one based on the application of the independent regions (dashed), for different values of the coupling A .

is hard to establish, since in a real setup not all scans are equal (like the $y_{i\ell}$ in the toy example) and the precision of each the measurement grows with the time invested in collecting the data. For instance, a procedure that is less sensitive but, on average, requires less scans to reach a conclusion (discovery/no discovery) allows researchers to redistribute the “extra time” to make fewer, but more precise, measurements. On this note, a procedure that reduces, at least on average, the number of scans needed is expected to be particularly impactful in view of future axion detectors, such as ALPHA [36], where the projected number of frequencies to be tested is on the order of 10^7 .

Finally, the CPU time required by each procedure is also non-negligible in practical applications. In this respect, calibrating the number of independent-regions, R_T^α , via Monte Carlo, requires approximately one order of magnitude more of CPU time than estimating the quantile $\mathcal{S}_{1-\alpha}$ in (36). For instance, in our example, computing each point in Figure 8 takes the same amount of time needed to estimate $\mathcal{S}_{1-\alpha}$. Although not relevant in terms of statistical properties, the computational complexity may become a decisive factor when dealing with real data.

For all the above-mentioned reasons, what represents “the best strategy” strictly depends on the experimental conditions as well as on the time and computational resources available. In light of this, the development of a solution which is optimal with respect to both the number of rescans and the CPU

time, while adjusting for the LEE, is left for future work.

5. Application on upper limits

A straightforward application of the proposed framework to a real detector is when setting upper limits, i.e., the case when no significant signal is detected and thus, the outcome of the experiment is the exclusion of the couplings that would have likely generated a signal. This application is particularly useful when dealing when projecting the reach of future experiments, for which no data has yet to be produced. To ease the intuition, let's consider once again the one scan-only framework of Section 3. To account for the possibility that a signal with some coupling A is present, the test statistic in (5) can be reformulated as

$$s(A) = \sqrt{u} \left(\frac{x}{u} - A \right) \quad (38)$$

and is distributed as a standard normal random variable. For a given observed value, $\hat{s}(A)$, of (38), the upper limit for the coupling, A_{UL} , is the value of A that solves

$$\Phi(\hat{s}(A)) = \alpha_{\text{UL}}, \quad (39)$$

with α_{UL} being desired significance at which we aim to set our upper limit (e.g., $\alpha_{\text{UL}} = 0.1$ for a 90% upper limit). Since $\Phi(\cdot)$ is the distribution of a standard Gaussian, Equation (39) can be easily inverted. The resulting upper limit for A is then

$$A_{\text{UL}} = \frac{\hat{x}/\sqrt{u} - \Phi^{-1}(\alpha_{\text{UL}})}{\sqrt{u}}. \quad (40)$$

This result is similar to what already found in [27]. Equation (40) can be further simplified when dealing with projected values of \hat{x} in view of future experiments rather than actual measured data. In this case, we expect to measure a null power excess ($\hat{x} = 0$). This gives an analytical formula which is statistically justified and can be easily applied — see e.g. [36].

In the remaining of this section, we demonstrate the validity of Equation (40) by comparing the resulting upper limit with the outcome of an analysis based on actual data. We will refer to the first run of HAYSTAC detector as presented in Refs. [31, 32]. Although the detector has been updated and newer results have been produced since then — see e.g. [41] — Ref. [32] is sufficiently detailed, in terms of general properties and data acquisition, to produce meaningful results.

Given its specifics, the experiment is designed to probe the frequency range [5.7, 5.8] GHz. The search is performed sequentially tuning the resonance of the

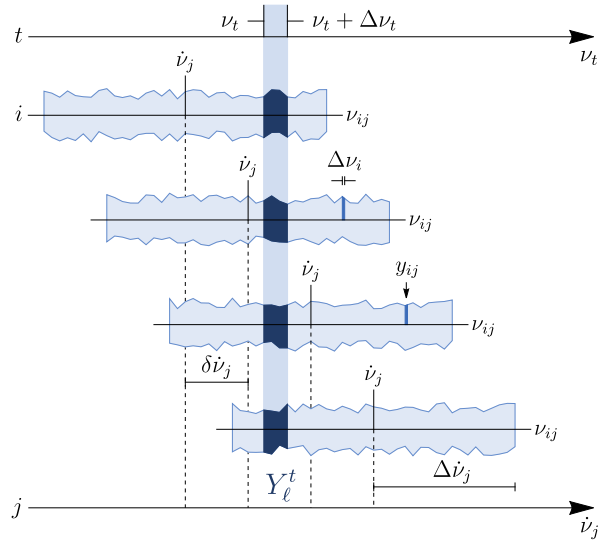


Figure 11: Sketch of the spectra, data format and relevant quantities for a HAYSTAC-like experiment.

cavity $\dot{\nu}_j$ at steps $\delta \dot{\nu}_j = 75$ kHz. Following our notation, the subscript j indexes the resonance of a given detector configuration and characterized by different values of its relevant parameters; for instance, the loaded quality factor Q_j (see also Figure 5.13 of [32]).

At each configuration, the detector is sensitive to the range of frequencies $\nu_{ij} \in [\dot{\nu}_j - \dot{\nu}_j/Q_j, \dot{\nu}_j + \dot{\nu}_j/Q_j]$; the latter correspond to the overlapping spectra in Figure 11. We denote with ν_{ij} the i -th frequency probed in the j -th configuration. Once a resonance is set, the power coming from a linear amplifier is measured for a total time $\tau_j = 15$ min, and is averaged over the time τ_{ij} needed to reach the frequency resolution $\Delta \nu_{ij} = 1/\tau_{ij} = 100$ Hz. In the real data acquisition, the whole range is scanned twice, “followed by several shorter scans to compensate for nonuniform tuning” (see [32], Figure 6.7). In order to collect a reasonable amount of data for the following calculations, we rely on Section 4.3.5 of the same reference and assume that the frequency range has been scanned exactly 3 times. In other words, each spectrum in Figure 11 comes in triplets or, conversely, we can imagine to deal with spectra acquired for $\tau_j = 45$ min.

The averaged measured powers in each spectrum can be shifted and rescaled with respect to their mean baseline, leading to adimensional quantities (see for instance Figure 2(c) in [35]). The resulting power fluctuations correspond to our y_{ij} in Equation (1) and constitute the data sample used in our analysis (without any further scaling and/or rebinning). The stan-

standard deviation of each fluctuation y_{ij} is

$$\sigma_{ij} = \sqrt{\frac{\tau_{ij}}{\tau_j}} = \frac{1}{\sqrt{\tau_j \Delta\nu_{ij}}}. \quad (41)$$

Whereas, their mean expresses the signal-to-noise ratio and can be factorized as (2). Here, A is an alias of the physical coupling constant between an axion and two photons, i.e. $A = g_{a\gamma\gamma}^2$. Note that, in natural units, $g_{a\gamma\gamma}$ is usually expressed in eV^{-1} . The factor w_{ij}^t is nonzero only if the axion at frequency t deposits power on the i -th bin of the j -th spectrum. Explicitly:

$$w_{ij}^t = \frac{P_j(\nu_t) \sqrt{\tau_{ij}/\Delta\nu_{ij}}}{h\nu_j N_{\text{sys}}(\nu_j, \nu_{ij})} D(\nu_t, \nu_j) L(\nu_t, \nu_{ij}). \quad (42)$$

The parameterization of each term follows from Ref. [32]. Specifically, P_j is the power per unit coupling constant (4.31), N_{sys} are the noise quanta (Figure 6.9 in [32]), $D(\nu_t, \nu_j)$ as in Equation (5.2) of [32] accounts for the possible mismatch between ν_j and ν_t , while $L(\nu_t, \nu_{ij})$ is the integral of the signal lineshape as in Equation (7.13) of [32] between each bin's edges. That is, since $\Delta\nu_t = 10^{-6}\nu_t \gg \Delta\nu_{ij}$, it quantifies the amount of signal falling in the bin.

Once the frequency ν_t to be tested has been selected, we can calculate the quantity u^t in (6) by collecting the measurements obtained over the bins in the spectrum that falls within the range $\nu_t \leq \nu_{ij} \leq \nu_t + \Delta\nu_t$. We can then compute Equation (40) with $\hat{x} = 0$ to obtain the projection of the 95% upper limit. The latter corresponds to the solid blue line in Figure 12. On the other hand, if we chose to define the upper limit with respect to the threshold value for a statistical discovery, $s_{5\sigma} = 5$, we would end up with a result about a factor 1.45 higher, as shown in Figure 12 as dashed blue line. The definition of the upper limit in terms of a threshold value is the same as that adopted in Ref. [32]. Their result is also shown in Figure 12 as a gray curve. The results are quite compatible, even if our computation relies on many simplifications and parameterizations of time-dependent value describing the detector properties.

6. Conclusions

In this paper, we have presented an inferential framework for axion searches that is statistically valid even when the experimental setup involves repeated scans. In Section 2, we have introduced the test statistic which is at the core of the likelihood-based rescan protocol discussed in Section 3.2 and is summarized in Figure 2. Specifically, when several scans are performed sequentially, our test statistic and the corresponding discovery thresholds are updated with as

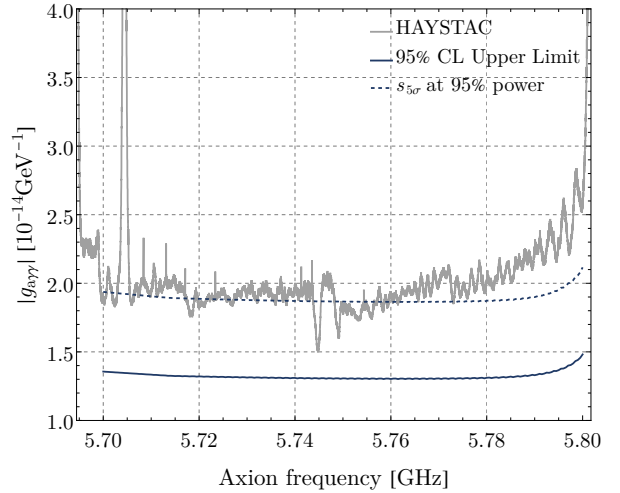


Figure 12: Upper limit projections for the first run of HAYSTAC detector originally presented in Refs. [31, 32] (gray line). Blue solid line: 95% upper limit from Equation (40) with $\hat{x} = 0$. Dashed line: limit given by $s_{5\sigma} = 5$ at 95% power.

new sets of data are collected, until the fluctuation is reabsorbed or a statistical discovery is claimed. An important feature of the proposed procedure is that, when the analysis is performed at a fixed frequency, one can compute the power and the statistical significance analytically. Adequate comparisons with the so-called geometric approach have been conducted in Section 3.3 and have shown that the likelihood-based inference enjoys higher power and, on average, a lower number of scans. Moreover, the likelihood-based inference provides a higher freedom in the definition of relevant quantities for data-acquisition. For instance, when the significance α and the maximum number of scans k_α have been set, the threshold x_{thr} in (13) is automatically determined and so is the rescan probability p_0 . On the other hand, the likelihood-based approach allows for more freedom in specifying p_0 given α and k_α fixed, as one can tune the constants b_ℓ and c_ℓ in Equations (25)–(26) to achieve the desired significance.

Another important contribution of this work is the introduction of adequate corrections for look-elsewhere effect, and required when testing multiple axion frequencies ν_t . Specifically, in Section 4, we have discussed Bonferroni and Sidak's correction based on the effective number of independent regions, and we have introduced a novel alternative solution that is meant to ease the burden of the Monte Carlo tuning. The two approaches have been compared in Section 4.1 by means of a toy example. The latter has shown that, while the method based on the independent re-

gions is characterized by a higher power, it is also requires, on average, a higher number of scans per outcome and discovery. It has to be noted, however, that establishing a direct comparison between the two in a real setup is a non-trivial task due to the interplay between the number of tested frequencies, the time spent measuring and the reachable precision of each measurement. An in-depth study of the performance of the different approaches when applied to real experiments is of paramount importance and paves the way to future improvements of this work.

Finally, in Section 5, we used our frequentist likelihood-based framework to reproduce a raw projection of the upper limit reachable by a realistic axion run in a real detector, as the phase one of HAYSTAC.

Acknowledgments

AGR and JC have been supported by a grant of the Knut and Alice Wallenberg Foundation and the Swedish Research Council.

References

- [1] F. Zwicky. “On the Masses of Nebulae and of Clusters of Nebulae”. In: *Astrophys. J.* 86 (1937), pp. 217–246. DOI: [10.1086/143864](https://doi.org/10.1086/143864).
- [2] L. Bergström. “Nonbaryonic dark matter: Observational evidence and detection methods”. In: *Rept. Prog. Phys.* 63 (2000), p. 793. DOI: [10.1088/0034-4885/63/5/2r3](https://doi.org/10.1088/0034-4885/63/5/2r3). arXiv: [hep-ph/0002126](https://arxiv.org/abs/hep-ph/0002126).
- [3] G. Bertone, D. Hooper, and J. Silk. “Particle dark matter: Evidence, candidates and constraints”. In: *Phys. Rept.* 405 (2005), pp. 279–390. DOI: [10.1016/j.physrep.2004.08.031](https://doi.org/10.1016/j.physrep.2004.08.031). arXiv: [hep-ph/0404175](https://arxiv.org/abs/hep-ph/0404175).
- [4] J. Jaeckel and A. Ringwald. “The Low-Energy Frontier of Particle Physics”. In: *Ann. Rev. Nucl. Part. Sci.* 60 (2010), pp. 405–437. DOI: [10.1146/annurev.nucl.012809.104433](https://doi.org/10.1146/annurev.nucl.012809.104433). arXiv: [1002.0329](https://arxiv.org/abs/1002.0329) [[hep-ph](https://arxiv.org/abs/hep-ph)].
- [5] J. L. Feng. “Dark Matter Candidates from Particle Physics and Methods of Detection”. In: *Ann. Rev. Astron. Astrophys.* 48 (2010), pp. 495–545. DOI: [10.1146/annurev-astro-082708-101659](https://doi.org/10.1146/annurev-astro-082708-101659). arXiv: [1003.0904](https://arxiv.org/abs/1003.0904) [[astro-ph](https://arxiv.org/abs/astro-ph).[C0](https://arxiv.org/abs/C0)].
- [6] S. Profumo, L. Giani, and O. F. Piattella. “An Introduction to Particle Dark Matter”. In: *Universe* 5.10 (2019), p. 213. DOI: [10.3390/universe5100213](https://doi.org/10.3390/universe5100213). arXiv: [1910.05610](https://arxiv.org/abs/1910.05610) [[hep-ph](https://arxiv.org/abs/hep-ph)].
- [7] A. Arbey and F. Mahmoudi. “Dark matter and the early Universe: a review”. In: *Prog. Part. Nucl. Phys.* 119 (2021), p. 103865. DOI: [10.1016/j.pnpnp.2021.103865](https://doi.org/10.1016/j.pnpnp.2021.103865). arXiv: [2104.11488](https://arxiv.org/abs/2104.11488) [[hep-ph](https://arxiv.org/abs/hep-ph)].
- [8] D. Green et al. “Snowmass Theory Frontier: Astrophysics and Cosmology”. In: (Sept. 2022). arXiv: [2209.06854](https://arxiv.org/abs/2209.06854) [[hep-ph](https://arxiv.org/abs/hep-ph)].
- [9] R. D. Peccei and H. R. Quinn. “CP Conservation in the Presence of Instantons”. In: *Phys. Rev. Lett.* 38 (1977), pp. 1440–1443. DOI: [10.1103/PhysRevLett.38.1440](https://doi.org/10.1103/PhysRevLett.38.1440).
- [10] R. D. Peccei and H. R. Quinn. “Constraints Imposed by CP Conservation in the Presence of Instantons”. In: *Phys. Rev. D* 16 (1977), pp. 1791–1797. DOI: [10.1103/PhysRevD.16.1791](https://doi.org/10.1103/PhysRevD.16.1791).
- [11] S. Weinberg. “A New Light Boson?” In: *Phys. Rev. Lett.* 40 (1978), pp. 223–226. DOI: [10.1103/PhysRevLett.40.223](https://doi.org/10.1103/PhysRevLett.40.223).
- [12] F. Wilczek. “Problem of Strong P and T Invariance in the Presence of Instantons”. In: *Phys. Rev. Lett.* 40 (1978), pp. 279–282. DOI: [10.1103/PhysRevLett.40.279](https://doi.org/10.1103/PhysRevLett.40.279).
- [13] J. Preskill, M. B. Wise, and F. Wilczek. “Cosmology of the Invisible Axion”. In: *Phys. Lett. B* 120 (1983). Ed. by M. A. Srednicki, pp. 127–132. DOI: [10.1016/0370-2693\(83\)90637-8](https://doi.org/10.1016/0370-2693(83)90637-8).
- [14] L. F. Abbott and P. Sikivie. “A Cosmological Bound on the Invisible Axion”. In: *Phys. Lett. B* 120 (1983). Ed. by M. A. Srednicki, pp. 133–136. DOI: [10.1016/0370-2693\(83\)90638-X](https://doi.org/10.1016/0370-2693(83)90638-X).
- [15] M. Dine and W. Fischler. “The Not So Harmless Axion”. In: *Phys. Lett. B* 120 (1983). Ed. by M. A. Srednicki, pp. 137–141. DOI: [10.1016/0370-2693\(83\)90639-1](https://doi.org/10.1016/0370-2693(83)90639-1).
- [16] L. Di Luzio et al. “The landscape of QCD axion models”. In: *Phys. Rept.* 870 (2020), pp. 1–117. DOI: [10.1016/j.physrep.2020.06.002](https://doi.org/10.1016/j.physrep.2020.06.002). arXiv: [2003.01100](https://arxiv.org/abs/2003.01100) [[hep-ph](https://arxiv.org/abs/hep-ph)].
- [17] K. Choi, S. H. Im, and C. Sub Shin. “Recent Progress in the Physics of Axions and Axion-Like Particles”. In: *Ann. Rev. Nucl. Part. Sci.* 71 (2021), pp. 225–252. DOI: [10.1146/annurev-nucl-120720-031147](https://doi.org/10.1146/annurev-nucl-120720-031147). arXiv: [2012.05029](https://arxiv.org/abs/2012.05029) [[hep-ph](https://arxiv.org/abs/hep-ph)].
- [18] F. Chadha-Day, J. Ellis, and D. J. E. Marsh. “Axion dark matter: What is it and why now?” In: *Sci. Adv.* 8.8 (2022), abj3618. DOI: [10.1126/sciadv.abj3618](https://doi.org/10.1126/sciadv.abj3618). arXiv: [2105.01406](https://arxiv.org/abs/2105.01406) [[hep-ph](https://arxiv.org/abs/hep-ph)].

- [19] P. W. Graham et al. “Experimental Searches for the Axion and Axion-Like Particles”. In: *Ann. Rev. Nucl. Part. Sci.* 65 (2015), pp. 485–514. DOI: [10.1146/annurev-nucl-102014-022120](https://doi.org/10.1146/annurev-nucl-102014-022120). arXiv: [1602.00039](https://arxiv.org/abs/1602.00039) [hep-ex].
- [20] I. G. Irastorza and J. Redondo. “New experimental approaches in the search for axion-like particles”. In: *Prog. Part. Nucl. Phys.* 102 (2018), pp. 89–159. DOI: [10.1016/j.pnpnp.2018.05.003](https://doi.org/10.1016/j.pnpnp.2018.05.003). arXiv: [1801.08127](https://arxiv.org/abs/1801.08127) [hep-ph].
- [21] J. Billard et al. *Direct Detection of Dark Matter – APPEC Committee Report*. Tech. rep. APPEC, Apr. 2021. arXiv: [2104.07634](https://arxiv.org/abs/2104.07634) [hep-ex].
- [22] I. G. Irastorza. “An introduction to axions and their detection”. In: *SciPost Phys. Lect. Notes* 45 (2022), p. 1. DOI: [10.21468/SciPostPhysLectNotes.45](https://doi.org/10.21468/SciPostPhysLectNotes.45). arXiv: [2109.07376](https://arxiv.org/abs/2109.07376) [hep-ph].
- [23] Y. K. Semertzidis and S. Youn. “Axion dark matter: How to see it?” In: *Sci. Adv.* 8.8 (2022), abm9928. DOI: [10.1126/sciadv.abm9928](https://doi.org/10.1126/sciadv.abm9928). arXiv: [2104.14831](https://arxiv.org/abs/2104.14831) [hep-ph].
- [24] C. B. Adams et al. “Axion Dark Matter”. In: *2022 Snowmass Summer Study*. Mar. 2022. arXiv: [2203.14923](https://arxiv.org/abs/2203.14923) [hep-ex].
- [25] P. Sikivie. “Detection Rates for ‘Invisible’ Axion Searches”. In: *Phys. Rev. D* 32 (1985). [Erratum: *Phys.Rev.D* 36, 974 (1987)], p. 2988. DOI: [10.1103/PhysRevD.36.974](https://doi.org/10.1103/PhysRevD.36.974).
- [26] H. Primakoff. “Photoproduction of neutral mesons in nuclear electric fields and the mean life of the neutral meson”. In: *Phys. Rev.* 81 (1951), p. 899. DOI: [10.1103/PhysRev.81.899](https://doi.org/10.1103/PhysRev.81.899).
- [27] J. W. Foster, N. L. Rodd, and B. R. Safdi. “Revealing the Dark Matter Halo with Axion Direct Detection”. In: *Phys. Rev. D* 97.12 (2018), p. 123006. DOI: [10.1103/PhysRevD.97.123006](https://doi.org/10.1103/PhysRevD.97.123006). arXiv: [1711.10489](https://arxiv.org/abs/1711.10489) [astro-ph.CO].
- [28] S. Knirck et al. “Directional axion detection”. In: *JCAP* 11 (2018), p. 051. DOI: [10.1088/1475-7516/2018/11/051](https://doi.org/10.1088/1475-7516/2018/11/051). arXiv: [1806.05927](https://arxiv.org/abs/1806.05927) [astro-ph.CO].
- [29] D. A. Palken et al. “Improved analysis framework for axion dark matter searches”. In: *Phys. Rev. D* 101.12 (2020), p. 123011. DOI: [10.1103/PhysRevD.101.123011](https://doi.org/10.1103/PhysRevD.101.123011). arXiv: [2003.08510](https://arxiv.org/abs/2003.08510) [astro-ph.IM].
- [30] S. Ahn et al. “Improved axion haloscope search analysis”. In: *JHEP* 04 (2021), p. 297. DOI: [10.1007/JHEP04\(2021\)297](https://doi.org/10.1007/JHEP04(2021)297). arXiv: [2004.08011](https://arxiv.org/abs/2004.08011) [astro-ph.CO].
- [31] B. M. Brubaker et al. “First results from a microwave cavity axion search at $24 \mu\text{eV}$ ”. In: *Phys. Rev. Lett.* 118.6 (2017), p. 061302. DOI: [10.1103/PhysRevLett.118.061302](https://doi.org/10.1103/PhysRevLett.118.061302). arXiv: [1610.02580](https://arxiv.org/abs/1610.02580) [astro-ph.CO].
- [32] B. M. Brubaker. “First results from the HAYSTAC axion search”. PhD thesis. Yale U., 2017. arXiv: [1801.00835](https://arxiv.org/abs/1801.00835) [astro-ph.CO].
- [33] S. J. Asztalos et al. “Large scale microwave cavity search for dark matter axions”. In: *Phys. Rev. D* 64 (2001), p. 092003. DOI: [10.1103/PhysRevD.64.092003](https://doi.org/10.1103/PhysRevD.64.092003).
- [34] C. Bartram et al. “Axion dark matter experiment: Run 1B analysis details”. In: *Phys. Rev. D* 103.3 (2021), p. 032002. DOI: [10.1103/PhysRevD.103.032002](https://doi.org/10.1103/PhysRevD.103.032002). arXiv: [2010.06183](https://arxiv.org/abs/2010.06183) [astro-ph.CO].
- [35] B. M. Brubaker et al. “HAYSTAC axion search analysis procedure”. In: *Phys. Rev. D* 96.12 (2017), p. 123008. DOI: [10.1103/PhysRevD.96.123008](https://doi.org/10.1103/PhysRevD.96.123008). arXiv: [1706.08388](https://arxiv.org/abs/1706.08388) [astro-ph.IM].
- [36] A. J. Millar et al. “ALPHA: Searching For Dark Matter with Plasma Haloscopes”. In: (Sept. 2022). arXiv: [2210.00017](https://arxiv.org/abs/2210.00017) [hep-ph].
- [37] J. L. Jensen. “The modified signed likelihood statistic and saddlepoint approximations”. In: *Biometrika* 79.4 (1992), pp. 693–703.
- [38] S. Algeri et al. “On methods for correcting for the look-elsewhere effect in searches for new physics”. In: *JINST* 11.12 (2016), P12010. DOI: [10.1088/1748-0221/11/12/P12010](https://doi.org/10.1088/1748-0221/11/12/P12010). arXiv: [1602.03765](https://arxiv.org/abs/1602.03765) [physics.data-an].
- [39] E. Gross and O. Vitells. “Trial factors for the look elsewhere effect in high energy physics”. In: *The European Physical Journal C* 70.1 (2010), pp. 525–530.
- [40] S. Algeri and D. A. van Dyk. “Testing One Hypothesis Multiple Times: The Multidimensional Case”. In: *Journal of Computational and Graphical Statistics* 29.2 (2020), pp. 358–371.
- [41] K. M. Backes et al. “A quantum-enhanced search for dark matter axions”. In: *Nature* 590.7845 (2021), pp. 238–242. DOI: [10.1038/s41586-021-03226-7](https://doi.org/10.1038/s41586-021-03226-7). arXiv: [2008.01853](https://arxiv.org/abs/2008.01853) [quant-ph].